



Published in final edited form as:

Nat Methods. 2015 March ; 12(3): 244–250. doi:10.1038/nmeth.3256.

A general method to improve fluorophores for live-cell and single-molecule microscopy

Jonathan B. Grimm¹, Brian P. English¹, Jiji Chen¹, Joel P. Slaughter¹, Zhengjian Zhang¹, Andrey Revyakin^{1,2}, Ronak Patel¹, John J. Macklin¹, Davide Normanno^{1,3}, Robert H. Singer^{1,4}, Timothée Lionnet¹, and Luke D. Lavis¹

¹Janelia Research Campus, Howard Hughes Medical Institute, Ashburn, VA, USA

²Department of Biochemistry, University of Leicester, Leicester, UK

³Laboratoire Physico-Chimie Curie, Institut Curie, Paris, France

⁴Department of Anatomy and Structural Biology, Albert Einstein College of Medicine, Bronx, NY, USA

Abstract

Specific labeling of biomolecules with bright fluorophores is the keystone of fluorescence microscopy. Genetically encoded self-labeling tag proteins can be coupled to synthetic dyes inside living cells, resulting in brighter reporters than fluorescent proteins. Intracellular labeling using these techniques requires cell-permeable fluorescent ligands, however, limiting utility to a small number of classic fluorophores. Here, we describe a simple structural modification that improves the brightness and photostability of dyes while preserving spectral properties and cell permeability. Inspired by molecular modeling, we replaced the *N,N*-dimethylamino substituents in tetramethylrhodamine with four-membered azetidine rings. This addition of two carbon atoms doubles the quantum efficiency and improves the photon yield of the dye in applications ranging from *in vitro* single-molecule measurements to super-resolution imaging. The novel substitution is generalizable, yielding a palette of chemical dyes with improved quantum efficiencies that spans the UV and visible range.

Users may view, print, copy, and download text and data-mine the content in such documents, for the purposes of academic research, subject always to the full Conditions of use:http://www.nature.com/authors/editorial_policies/license.html#terms

Corresponding authors: Timothée Lionnet (lionnett@janelia.hhmi.org) and Luke D. Lavis (lavisl@janelia.hhmi.org).

Author Contributions

J.B.G conceived the project and performed organic synthesis. B.P.E. and J.C. designed and performed cellular microscopy experiments. J.P.S performed organic synthesis. Z.Z. prepared bioconjugates, performed *in vitro* single-molecule microscopy, and analyzed data. A.R. performed *in vitro* single-molecule microscopy and analyzed data. R.P. and J.J.M. performed two-photon spectroscopy and fluorescence lifetime measurements. D.N. designed and validated the SnapTag–TetR plasmid. R.H.S. interpreted data. T.L. designed experiments and performed data analysis. L.D.L. conceived the project, performed one-photon spectroscopic measurements, and wrote the manuscript with input from the other authors.

Competing Interests

The authors declare competing interests: patent applications have been filed whose value may be affected by this publication.

Introduction

Fluorescence imaging of specific intracellular molecules requires precise labeling with bright, photostable fluorophores. Genetically encoded fluorophores (green fluorescent protein, GFP, and variants) excel with regard to their genetic specificity of labeling,¹ but lack the requisite photostability for single-molecule microscopy and other photon-intensive imaging paradigms.² Over the past two decades, a number of alternative labeling strategies have been developed that combine the genetic specificity of fluorescent proteins with the favorable photophysics of small molecule fluorophores. These include FIAsh,³ enzyme-based “self-labeling tags” (*e.g.*, SnapTag⁴ and HaloTag^{5,6}), electrophilic ligand–receptor pairs (*e.g.*, TMPTag⁷ and coumarin–PYP⁸), and lipoic acid ligase variants.⁹ In particular, the self-labeling tags have enabled advanced imaging experiments inside living cells such as super-resolution microscopy^{7,10,11} and biomolecular tracking at single-molecule resolution.^{12,13}

Although the general collection of chemical dyes is extensive,^{14–16} relatively few exhibit the cell permeability needed for intracellular labeling. Thus, the available palette of intracellular self-labeling tag ligands has been limited to classic, net neutral fluorophores based on coumarin and rhodamine scaffolds,^{4–6,17,18} which exhibit excellent membrane permeability and rapid labeling kinetics, but suboptimal brightness and photostability. Previous campaigns to improve dye performance (*e.g.*, Cy, Alexa Fluor), involved substantial modifications such as structural rigidification and addition of sulfonate groups.^{19–21} These efforts resulted in highly polar, cell-impermeant dyes, useful *in vitro*²² or on the cell exterior,²³ but incompatible with live-cell intracellular applications.

We sought, and now report, a general strategy to improve the brightness of fluorophores through a minimal structural change, thereby preserving cell permeability and efficiency of intracellular labeling. Based on molecular modeling, we replaced the *N,N*-dimethyl group in the classic dye tetramethylrhodamine (TMR) with a four-membered azetidine ring. This minor alteration—a net addition of two carbon atoms—elicited a large increase in quantum yield relative to the parent fluorophore, enabling prolonged observations of single molecules in tracking experiments and localization microscopy with improved spatial resolution. We expanded this strategy to other fluorophores including the coumarin, naphthalimide, acridine, rhodol, carborhodamine, oxazine, and silarhodamine classes, where the straightforward replacement of *N,N*-dialkylamino groups with azetidines also increased quantum yield. This general method represents a marked advance in the chemistry of synthetic labels for biological imaging, allowing substantial improvements in brightness while preserving the requisite small size and high membrane permeability for use in live cells.

Results

Rational design of an improved tetraalkylrhodamine dye

The simplest rhodamine fluorophore, rhodamine 110 (**1**, Fig. 1a), exhibits an absorption maximum in the blue ($\lambda_{\text{max}} = 497 \text{ nm}$) with a large extinction coefficient ($\epsilon = 7.6 \times 10^4 \text{ M}^{-1}\text{cm}^{-1}$), emission in the green ($\lambda_{\text{em}} = 520 \text{ nm}$), and a high quantum yield ($\Phi = 0.88$).²⁴

Alkylation of the rhodamine elicits a bathochromic shift in absorption and fluorescence emission wavelengths. For example, TMR (**2**) displays $\lambda_{\max}/\lambda_{\text{em}} = 548 \text{ nm}/572 \text{ nm}$ and $\epsilon = 7.8 \times 10^4 \text{ M}^{-1}\text{cm}^{-1}$ (Fig. 1a). This shift in spectral properties is accompanied by a large decrease in quantum yield, with TMR showing $\Phi = 0.41$ in aqueous solution. Both of these dyes are used in commercial self-labeling tag substrates and can be used to label intracellular and extracellular proteins in living cells.

A plausible explanation for the lower quantum efficiency of *N,N,N',N'*-tetraalkylrhodamines such as **2** is the formation of a twisted internal charge transfer (TICT) state. In this process fluorophore **2** absorbs a photon to give an excited state (**2***, Fig. 1b), followed by electron transfer from the nitrogen atom to the xanthen ring system with concomitant twisting of the $\text{C}_{\text{aryl}}\text{-N}$ bond (**2_{TICT}**). TICT is energetically favorable in tetraalkylrhodamine dyes due to the lower ionization potential of *N,N*-dialkylanilines *versus* less substituted anilines.²⁵ The TICT form relaxes without emission of a photon leading to rapid nonradiative decay of the excited state.^{25–27} The **2_{TICT}** diradical intermediate may also undergo irreversible bleaching reactions.²⁷ Thus, rhodamine derivatives where TICT is disfavored should exhibit increased quantum efficiency, longer fluorescence lifetimes, and higher photostability.

Based on this hypothesis, we reasoned that replacing the *N,N*-dimethyl group in TMR (**2**) with different sized nitrogen-containing rings (ranging from aziridine to azepane, compounds **3–7**, Fig. 1a) might mitigate TICT and improve fluorescent properties. Although previous work had shown the pyrrolidine-containing rhodamine **5** to have a higher fluorescence brightness than the piperidino-rhodamine **6**,^{25,28} azacyclic-rhodamines with smaller or larger ring sizes (**3**, **4**, and **7**) had not been explored. Based on quantum mechanical calculations, we predicted that the novel azetidiny-rhodamine **4** would exhibit superior brightness to TMR (**2**) and the other alkylated rhodamines **3**, **5**, **6** and **7** (Supplementary Note).

To test this prediction we synthesized compounds **3–7** from fluorescein (**8**) using a Pd-catalyzed cross-coupling approach (Fig. 1c, Supplementary Note).²⁸ We then evaluated the photophysical properties of compounds **3–7** in aqueous solution, comparing them to known rhodamines **1** and **2** (Fig. 1a, Supplementary Fig. 1a). Aziridine derivative **3** gave a colorless solution with no discernible fluorescence, suggesting the ring strain in the aziridine substituents forces the rhodamine molecule to adopt a colorless, nonfluorescent lactone form. Compounds **4–7** showed λ_{\max} and λ_{em} values similar to TMR (**2**) with increased ring size causing a slight bathochromic shift of up to 10 nm. Compounds **4** and **7** showed a ~30% higher extinction coefficient than the other dyes; values of this magnitude have been observed with tetraethylrhodamine.^{15,28}

Although the λ_{\max} , λ_{em} , and ϵ of the different rhodamine dyes showed only modest dependence on substituent ring size, the fluorescence lifetime (τ) and quantum yield (Φ) varied widely as a function of molecular structure (Fig. 1a). Rhodamine **4** exhibited a high quantum yield value ($\Phi = 0.88$) and long fluorescence lifetime ($\tau = 3.8 \text{ ns}$), larger than the values for TMR (**2**; $\Phi = 0.41$, $\tau = 2.2 \text{ ns}$), and similar to the parent rhodamine 110 (**1**; $\Phi = 0.88$, $\tau = 3.3 \text{ ns}$). Rhodamine **4** was also 60% brighter than the pyrrolidine derivative **5**, which showed $\Phi = 0.74$ and $\tau = 3.6 \text{ ns}$. The piperidine derivative **6** showed a sharp decrease

in fluorescence with $\Phi = 0.10$ and $\tau = 0.6$ ns; the lifetime values for **5** and **6** are consistent with those measured for similar fluorophores.²⁵ Rhodamine **7** gave slightly higher values of $\Phi = 0.25$ and $\tau = 1.62$ ns relative to **6**, suggesting that the increased flexibility of this larger ring can offset the other deleterious structural effects on rhodamine fluorescence.

The improved brightness of rhodamine **4** under one-photon excitation (Fig. 1a) extended to two-photon excitation (Fig. 1d, Supplementary Fig. 1b). This enhancement is brought about by a negligible structural change—the addition of two carbon atoms—that preserves many of the desirable properties of TMR. For example, the absorption and emission spectra of **2** and **4** are superimposable (Fig. 1e) and the dyes show comparable sensitivity to solvent polarity (Supplementary Fig. 1c), suggesting similar cell permeability.^{18,24} Based on its high brightness, favorable chemical properties, and $\lambda_{\text{max}} = 549$ nm, azetidinyrhodamine **4** was given the name “JF₅₄₉” (Janelia Fluor 549).

Utility of JF₅₄₉ in cellular imaging

To evaluate the performance of the dye as a label, we synthesized JF₅₄₉–HaloTag ligand (**9**, Fig. 1f) starting from a 6-carboxyfluorescein derivative (Supplementary Note). This molecule is a direct analog of the commercial TMR-based HaloTag ligand **10**. We compared the labeling kinetics of compounds **9** and **10** with a novel Cy3 HaloTag ligand, and measured the brightness and photon yield of the resulting conjugates. The JF₅₄₉ ligand (**9**) showed comparable labeling kinetics to the TMR ligand (**10**) and increased brightness relative to the other dyes (Supplementary Note). Incubation of live cells expressing a HaloTag–histone 2B (H2B) fusion with compound **9** resulted in bright nuclear labeling (Fig. 1g) and low cytoplasmic background, demonstrating that the JF₅₄₉ HaloTag ligand can efficiently cross the membrane of live cells and selectively label the HaloTag protein.

Incubation of **9** or **10** using low amounts of ligand (<50 nM) allowed imaging of single molecules (Supplementary Video 1) and evaluation of fluorophore brightness (photons/s) and photostability (*i.e.*, tracklength, s) of individual molecules of labeled HaloTag–H2B. The JF₅₄₉ ligand **9** demonstrated a large increase in both brightness and photostability compared to TMR ligand **10** (Fig. 1h). Proteins labeled with **10** showed average photons/s = 1.1×10^4 and a mean track length of 0.72 s. Conjugates of JF₅₄₉ ligand **9** emit nearly twice the number of photons/s (1.9×10^4) and last about twice as long (average track length = 1.6 s). This improvement in single molecule brightness extended to direct stochastic optical reconstruction microscopy experiments (*d*STORM), where the use of a reducing environment enables the reversible photoswitching of synthetic fluorophores.^{7,29–31} We labeled cells expressing HaloTag–H2B with JF₅₄₉ ligand **9** or TMR ligand **10**, followed by fixation and imaging using standard *d*STORM conditions. This resulted in a super-resolution image of H2B using ligand **9** (Fig. 1i) or molecule **10** (Supplementary Fig. 2a) with median localization errors (σ) of 14.1 nm and 17.0 nm, respectively (Supplementary Fig. 2b). We could also perform *d*STORM inside living cells using the cellular reducing environment to elicit photoswitching of the JF₅₄₉ label (Supplementary Fig. 2c).⁷ Together, our results establish JF₅₄₉ as the best available ligand in this spectral range for HaloTag conjugation *in vitro*, in fixed cells, and in live cells, validating our fluorophore design strategy.

Extension of the azetidine strategy to other dye scaffolds

Based on the improved brightness observed with the rhodamine scaffold, we sought to replace *N,N*-dialkyl groups found in other fluorophores with azetidines. The *N,N*-dialkyl motif is found in numerous classic fluorophore scaffolds (Table 1),¹⁴ including coumarins (e.g., **11**, Coumarin 461), naphthalimides, acridines (e.g., **17**, Acridine Orange), rhodols, carborhodamines,²⁴ oxazines (e.g., **23**, Oxazine 1), and silarhodamines.^{18,32} TICT has been proposed as a major contributor to nonradiative decay in these fluorescent systems, leading to modest quantum efficiencies.²⁶ As with the rhodamine case, we used an efficient Pd-catalyzed cross-coupling approach to install the azetidine motif in these fluorophores, starting from accessible aryl halides or aryl triflates (Supplementary Note).

In all cases the azetidine substitution imparted large increases in quantum yield without substantial deleterious effects on other spectral properties (Table 1, Supplementary Fig. 3). Coumarin 461 (**11**) exhibits $\lambda_{\max}/\lambda_{\text{em}} = 372 \text{ nm}/470 \text{ nm}$, $\epsilon = 1.8 \times 10^4 \text{ M}^{-1}\text{cm}^{-1}$, and a modest $\Phi = 0.19$ in aqueous buffer. The analog **12** shows a five-fold increase in quantum yield ($\Phi = 0.96$) along with an 18-nm hypsochromic shift in absorbance maxima ($\lambda_{\max} = 354 \text{ nm}$). The emission spectrum and extinction coefficient of **12** ($\lambda_{\max} = 467 \text{ nm}$, $\epsilon = 1.5 \times 10^4 \text{ M}^{-1}\text{cm}^{-1}$) were similar to the parent dye **11**. The widely used 7-(diethylamino)coumarin-3-carboxylic acid (DEAC, **13**) displays $\lambda_{\max}/\lambda_{\text{em}} = 410 \text{ nm}/471 \text{ nm}$, $\epsilon = 3.5 \times 10^4 \text{ M}^{-1}\text{cm}^{-1}$, but a low quantum yield ($\Phi = 0.03$). The azetidiny analog **14** showed a shorter absorption maximum ($\lambda_{\max} = 387 \text{ nm}$) and a smaller extinction coefficient ($\epsilon = 2.4 \times 10^4 \text{ M}^{-1}\text{cm}^{-1}$). Nonetheless, the emission maxima proved quite similar with $\lambda_{\text{em}} = 470 \text{ nm}$, and the azetidine substitution increased the quantum yield by almost 30-fold ($\Phi = 0.84$).

We then considered the naphthalimide, acridine, and rhodol fluorophore scaffolds. Dimethylamino-substituted naphthalimides such as compound **15** are important environmentally sensitive fluorophores,³³ but have not been useful as general fluorescent labels due to their poor absorbance and fluorescence in water ($\lambda_{\max} = 436 \text{ nm}$, $\epsilon = 9.5 \times 10^3 \text{ M}^{-1}\text{cm}^{-1}$, $\Phi < 0.01$, Table 1). We prepared the azetidiny analog **16**, which showed a bathochromic shift in absorbance maxima ($\lambda_{\max} = 464 \text{ nm}$), a larger extinction coefficient ($\epsilon = 1.8 \times 10^4 \text{ M}^{-1}\text{cm}^{-1}$), and a high quantum yield ($\Phi = 0.28$, $\lambda_{\text{em}} = 553 \text{ nm}$). The classic fluorophore Acridine Orange (**17**) gave $\Phi = 0.21$ when measured in aqueous solution, consistent with published data.³⁴ The azetidine analog **18** was 2.5-fold brighter with $\Phi = 0.52$. Other spectral properties of the two acridines were similar. Rhodol **19** showed $\lambda_{\max}/\lambda_{\text{em}} = 518 \text{ nm}/546 \text{ nm}$, and $\epsilon = 6.0 \times 10^4 \text{ M}^{-1}\text{cm}^{-1}$ and $\Phi = 0.21$, consistent with previous results.³⁵ The azetidine-containing analog **20** had nearly indistinguishable λ_{\max} , λ_{em} , and ϵ values. However, the replacement of the *N,N*-dimethylamino group in **19** with an azetidine in **20** gave a 4-fold increase in quantum yield ($\Phi = 0.85$).

We then turned to longer-wavelength fluorophores. The carbon-containing analog of tetramethylrhodamine (**21**) exhibited $\lambda_{\max}/\lambda_{\text{em}} = 606 \text{ nm}/626 \text{ nm}$, $\epsilon = 1.21 \times 10^5 \text{ M}^{-1}\text{cm}^{-1}$, and $\Phi = 0.52$ in aqueous buffer (Table 1). The azetidiny-carborhodamine **22** showed similar absorption and emission maxima ($\lambda_{\max}/\lambda_{\text{em}} = 608 \text{ nm}/631 \text{ nm}$) and extinction coefficient ($\epsilon = 9.9 \times 10^4 \text{ M}^{-1}\text{cm}^{-1}$), but a higher quantum yield ($\Phi = 0.67$). The classic dye Oxazine 1 (**23**) showed spectral properties in the far red with $\lambda_{\max}/\lambda_{\text{em}} = 655 \text{ nm}/669 \text{ nm}$ and $\epsilon = 1.11$

$\times 10^5 \text{ M}^{-1}\text{cm}^{-1}$, but a relatively low $\Phi = 0.07$. The azetidine substitution in dye **24** gave a small hypsochromic shift ($\lambda_{\text{max}}/\lambda_{\text{em}} = 647 \text{ nm}/661 \text{ nm}$), a slightly lower extinction coefficient ($\varepsilon = 9.9 \times 10^4 \text{ M}^{-1}\text{cm}^{-1}$), and a 3.4-fold improvement in quantum yield ($\Phi = 0.24$). Finally, the recently described silicon-containing TMR (SiTMR, **25**)^{18,32} showed $\lambda_{\text{max}}/\lambda_{\text{em}} = 643 \text{ nm}/662 \text{ nm}$ and $\Phi = 0.41$; the azetidiny analog **26** gave similar absorption and emission maxima ($\lambda_{\text{max}}/\lambda_{\text{em}} = 643 \text{ nm}/662 \text{ nm}$) and a higher $\Phi = 0.54$. Since silarhodamines often adopt a colorless form in water,^{18,32} we measured the extinction coefficients in acidic ethanol, finding $\varepsilon = 1.41 \times 10^5 \text{ M}^{-1}\text{cm}^{-1}$ for SiTMR (**25**) and $\varepsilon = 1.52 \times 10^5 \text{ M}^{-1}\text{cm}^{-1}$ for azetidine **26**. Overall, these results demonstrate that the azetidiny substitution is generalizable to different fluorophore scaffolds, producing substantial improvements in quantum yield values.

Cellular imaging using azetidiny silarhodamine

Compounds based on SiTMR (**25**) were previously reported to be efficient labels for the SnapTag, HaloTag, and other proteins inside live cells.^{18,32} Compound **26** exhibits superior brightness ($\varepsilon \times \Phi$, Table 1) relative to **25** and was given the name JF₆₄₆ (Janelia Fluor 646). To compare these two dyes directly in cellular imaging experiments we synthesized the HaloTag ligand of the azetidiny-silarhodamine (**27**, Fig. 2a) and the known¹⁸ HaloTag ligand of SiTMR (**28**), starting from a novel silafluorescein precursor (Supplementary Note). Both silarhodamine ligands **27** and **28** were excellent labels for super-resolution *d*STORM imaging of HaloTag–H2B (Fig. 2b, Supplementary Fig. 4a), showing median localization errors of 8.4 nm and 9.0 nm, respectively (Supplementary Fig. 4b). We also performed *d*STORM on live cells expressing HaloTag–tubulin and labeled with JF₆₄₆ ligand **27**. We observed excellent photon yields and low background with this label, giving a median $\sigma = 7.1 \text{ nm}$ (Supplementary Fig. 4c–e).

As noted above, the free silarhodamine dyes **25** and **26** exhibit low visible absorption in aqueous solution, suggesting that the dyes preferentially adopt the closed, UV-absorbing, lactone form. However, conjugation to a protein changes the local environment around the dye, eliciting a large increase in absorbance.^{18,32} We compared the chromogenicity of ligands **27** and **28** upon reaction with purified protein and in live-cell imaging experiments. The SiTMR ligand **28** showed an enhancement of 6.8-fold upon reaction with excess HaloTag protein in buffer (Fig. 2c), consistent with previous reports.¹⁸ The azetidiny-silarhodamine–HaloTag ligand **27** showed lower background, leading to a larger, 21-fold increase in absorbance under the same conditions (Fig. 2d). We then performed “no wash” imaging experiments using cells expressing the HaloTag–H2B fusion. Incubation with either ligand (100 nM) followed directly by wide-field imaging gave brightly labeled nuclei using both the SiTMR ligand **28** (Fig. 2e) and the JF₆₄₆ ligand **27** (Fig. 2f). However, SiTMR showed substantial extranuclear fluorescence (Fig. 2g), whereas the JF₆₄₆ ligand exhibited lower nonspecific staining (Fig. 2h, Supplementary Fig. 4f). Overall, these results show the known SiTMR ligand **28** can be replaced with the structurally similar JF₆₄₆ ligand **27** to achieve better localization error in super-resolution imaging and lower background in conventional fluorescence microscopy.

The excellent properties of JF₅₄₉ and JF₆₄₆ and the large spectral separation between the two fluorophores raised the possibility of imaging two distinct protein species at the single-molecule level in the same living cell. To achieve orthogonal labeling, we prepared the SnapTag ligand of JF₅₄₉ (**29**, Fig. 2i, Supplementary Note). We coexpressed HaloTag–H2B and a fusion of the SnapTag enzyme and the Tet repressor protein (SnapTag–TetR) and labeled the HaloTag–H2B with JF₆₄₆ ligand **27** and the SnapTag–TetR with JF₅₄₉ ligand **29**. We imaged the trajectories of individual JF₅₄₉-labeled TetR proteins followed by a rapid live-cell *d*STORM experiment of the JF₆₄₆–H2B conjugate (Supplementary Fig. 4g, Supplementary Video 2). This proof-of-concept, two-color experiment revealed the respective partitions of fast- and slow-diffusing DNA-binding protein in relation to the chromatin structure of the nucleus (Fig. 2j) and showed slowly diffusing TetR colocalized with H2B to a greater extent than with non-colocalized positions (Supplementary Fig. 4h), consistent with previous observations that inert tracers diffuse more slowly in dense chromatin regions.³⁶

Cellular imaging using an azetidiny-coumarin label

The improvements to coumarin **13** brought about by the azetidine substitution were also interesting, as derivatives of this cell-permeable dye can be used for intracellular labeling. We compared the performance of a commercial SnapTag ligand **30** (*i.e.*, Snap Cell 430; Fig. 3a) to a novel azetidiny derivative **31**, which we synthesized from coumarin **14** (Supplementary Note). Under identical transient transfection, labeling, and imaging conditions, H2B–SnapTag-expressing cells were stained with the red fluorescent nuclear stain DRAQ5 and either known ligand **30** or azetidiny ligand **31**. Using the DRAQ5 staining as a spatial reference (Fig. 3b, c) we measured the intensity of individual nuclei labeled by either SnapTag ligand. Cells incubated with ligand **30** showed low fluorescence intensity (Fig. 3d) whereas cells labeled with **31** showed brighter nuclear labeling (Fig. 3e). Quantification of nuclear intensity showed the cells labeled with azetidine **31** were on average five-fold higher than cells labeled with the commercial compound **30** (Fig. 3f).

Discussion

We report a simple structural modification—the replacement of *N,N*-dialkyl groups with azetidines—that improves the quantum efficiency of classic fluorophores with absorbance maxima from the UV to the far-red. In particular, the azetidine substitution endows JF₅₄₉ and JF₆₄₆ with superior brightness while retaining excellent cell penetration and fast labeling kinetics with the HaloTag. These novel dyes should facilitate new microscopic experiments such as multiplexed single-molecule measurements at a high spatiotemporal resolution inside living cells (*e.g.*, Fig. 2j). Such experiments will constitute a major tool in testing models relating molecular architecture and biological dynamics.^{36,37}

In addition to serving as ligands for self-labeling tags, many classic fluorophores are components of fluorescent labels, stains, and indicators.^{14,15,21} Replacement of the dialkylamino groups in these molecules with azetidines could yield a new generation of probes with improved properties. For example, derivatives of the bright coumarin fluorophores **12** and **14** could find use in other protein-based labeling schemes^{8,9} or as non-

natural amino acids,³⁸ where the size of the fluorophore label is restricted by the biochemical machinery. This general approach to attenuate nonradiative decay sets the stage for combinatorial enhancements via other structural modifications, such as halogenation³⁹ or attachment of triplet-state quenchers,⁴⁰ to further improve brightness and photostability, altogether pushing the limits of biological imaging.

Online Methods

General Spectroscopic Methods

Fluorescent and fluorogenic molecules for spectroscopy were prepared as stock solutions in DMSO and diluted such that the DMSO concentration did not exceed 1% v/v. Phosphate buffered saline (PBS) was at pH 7.4 unless otherwise noted. Commercial compounds for spectroscopy were of the highest quality available and obtained from the following sources: Exciton (**1**); Anaspec (**2**); Promega (**10**); Sigma–Aldrich (**11**, **13**); Life Technologies (**17**); AAT Bioquest (**23**); New England BioLabs (**30**).

UV–Vis and Fluorescence Spectroscopy

Spectroscopy was performed using 1-cm path length, 3.5-mL quartz cuvettes from Starna Cells or 1-cm path length, 1.0-mL quartz microcuvettes from Hellma. All measurements were taken at ambient temperature (22 ± 2 °C) in 10 mM HEPES, pH 7.3 buffer unless otherwise noted. Absorption spectra were recorded on a Cary Model 100 spectrometer (Varian); reported values for extinction coefficients (ϵ) are averages ($n = 3$). Fluorescence spectra were recorded on a Cary Eclipse fluorometer (Varian). Normalized spectra are shown for clarity.

Quantum Yield Determination

All reported quantum yield values were measured in our laboratory under identical conditions using a Quantaury-QY spectrometer (C11374, Hamamatsu). This instrument uses an integrating sphere to determine photons absorbed and emitted by a sample. Measurements were carried out using dilute samples ($A < 0.1$) and self-absorption corrections⁴¹ were performed using the instrument software. Reported values are averages ($n = 3$).

Dioxane–H₂O Titration

Dioxane–H₂O titrations were performed in spectral grade dioxane (Sigma–Aldrich) and milliQ H₂O. The solvent mixtures contained 0.01% v/v triethylamine to ensure the rhodamine dyes were in the zwitterionic form. The absorbance values at λ_{max} were measured on 5 μM samples ($n = 2$) using a quartz 96-well microplate (Hellma) and a FlexStation3 microplate reader (Molecular Devices). Values of dielectric constant (ϵ_r) were as reported.⁴²

Multiphoton-Photon Spectroscopy

The two-photon measurements were performed as previously described.^{43,44} Measurements were taken on an inverted microscope (IX81, Olympus) equipped with a 60 \times , 1.2NA water objective (Olympus). Dye samples were excited with pulses from an 80 MHz Ti-Sapphire

laser (Chameleon Ultra II, Coherent). Fluorescence collected by the objective was passed through a shortpass filter (720SP, Semrock) and a bandpass filter (550BP200, Semrock), and detected by a fiber-coupled Avalanche Photodiode (APD). Two different APDs were used, one optimized for low noise for FCS and spectral measurements (SPCM_AQRH-14, Perkin Elmer) and the other for precise timing for lifetime measurements (PDF-CCTB, Micro Photon Devices). The focused laser spot size was measured to be $0.420\ \mu\text{m}$ (radius where intensity drops to $1/e^2$). Two-photon excitation spectra were taken on samples of $1\ \mu\text{M}$ dye in HEPES buffer, using $1\ \text{mW}$ of laser power at the sample across the spectral range of 710 nm to 1080 nm. The peak molecular brightness, defined as the maximum detected count rate per emitting molecule, was obtained by determining the fluorescence count rate and the average number of emitting molecules in the beam using fluorescence correlation spectroscopy (FCS).⁴³ For FCS measurements, a stock dye solution was diluted to $50\ \text{nM}$ in $50\ \text{mM}$ HEPES, pH 7.2 and excited at discrete laser powers ranging from $5\text{--}30\ \text{mW}$, with FCS data acquisition for each power setting taken for $100\text{--}200\ \text{s}$. The samples were excited at $830\ \text{nm}$ and $1020\ \text{nm}$ laser wavelength (the absorption peaks obtained from two photon excitation spectra). The fluorescence signal detected by the APD at each wavelength and power setting was fed to the autocorrelator (Flex03LQ; Correlator.com) and a computer program recorded the autocorrelation function and average fluorescence counts per second, defined as $\langle F \rangle$. The measured autocorrelation curve was fit to an FCS diffusion model with a MATLAB program using a customized code,⁴³ to determine the average number of excited molecules $\langle N \rangle$ in the volume of excitation. The molecular brightness (ϵ) was thus obtained as the rate of fluorescence per excited molecule defined as $\epsilon = \langle F \rangle / \langle N \rangle$.⁴³ Increasing the laser intensity initially increases the molecular brightness, however at a certain point molecular brightness leveled off or started decreasing, indicating photobleaching or saturation of the molecule in the excitation volume. The maximum or peak brightness achieved before photobleaching or saturation represents the useful proxy for the photostability of a fluorophore.

Fluorescence Lifetime Spectroscopy

For fluorescence lifetime measurements, a pulse picker (Model 350-160, ConOptics) was placed in the laser beam to reduce the pulse frequency from $80\ \text{MHz}$ to $20\ \text{MHz}$. Samples ($2\ \mu\text{M}$ dye diluted in $50\ \text{mM}$ HEPES, pH 7.2, H_2O , or CH_3OH) were excited at $830\ \text{nm}$ laser wavelength and $6\ \text{mW}$ laser power. The emitted light was collected by the fast-timing APD and fed to the single-photon counting board (TimeHarp200; PicoQuant). Timing pulses were obtained from a PIN diode (DET01CFC; ThorLabs) monitoring the $20\ \text{MHz}$ pulse train. The temporal impulse response of the system was determined by second harmonic generation of laser pulses using a thin nonlinear crystal in place of a dye sample. The lifetime decay data was fit to a single exponential decay function using a custom MATLAB program. Lifetime value of the reference fluorescein dye measured using our system was $4.025 \pm 0.015\ \text{ns}$ ($R^2 = 0.99$) compared to a literature value of $4.1 \pm 0.1\ \text{ns}$.⁴⁵

Measurement of Increase in Fluorescence of HaloTag Ligands 27 and 28 Upon Reaction with HaloTag Protein

Absorbance measurements were performed in $1\ \text{mL}$ quartz cuvettes. HaloTag protein was used as a $100\ \mu\text{M}$ solution in $75\ \text{mM}$ NaCl, $50\ \text{mM}$ TRIS-HCl, pH 7.4 with 50% v/v glycerol

(TBS–glycerol). HaloTag ligands **27** and **28** (5 μM) were dissolved in 10 mM HEPES, pH 7.3 containing 0.1 $\text{mg}\cdot\text{mL}^{-1}$ CHAPS. An aliquot of HaloTag protein (1.5 equiv) or an equivalent volume of TBS–glycerol blank was added and the resulting mixture was incubated until consistent absorbance signal was observed (~30 min). Additional HaloTag protein did not elicit an increase in absorbance (not shown). Absorbance scans are averages ($n = 2$).

Cell Culture, Transfection, and Labeling

HeLa cells (ATCC) and U2OS cells (ATCC) were cultured in Dulbecco's modified eagle medium (DMEM; Life Technologies) supplemented with 10% v/v fetal bovine serum (FBS; Life Technologies), 1 mM GlutaMax (Life Technologies), and 1 mM sodium pyruvate (Sigma) and maintained at 37 °C in a humidified 5% v/v CO₂ environment. These cell lines undergo regular mycoplasma testing by the Janelia Cell Culture Facility. Cells were transfected with HaloTag–H2B, HaloTag–tubulin, SnapTag–TetR, or SnapTag–H2B using an Amaxa Nucleofector (Lonza). Before the imaging experiments, transfected cells were transferred onto a No.1 coverslip (Warner Instruments) that was cleaned by Piranha solution (3:1 v/v mixture of concentrated H₂SO₄ and 30% v/v hydrogen peroxide). To label live cells with the HaloTag or SnapTag ligands, compounds **9**, **10**, **27**, **28**, **29**, **30**, or **31** were added to the growth medium and the samples incubated for 15 min. Labeling concentrations were typically 100–500 nM for confocal, wide-field, and dSTORM experiments and 5–50 nM for single-molecule tracking experiments. Cells were then washed briefly with PBS (1 \times) and then incubated in DMEM–FBS for an additional 15 min. Before imaging, the cells were washed briefly with PBS (3 \times) and placed in fresh DMEM–FBS for imaging. All washes were omitted in the “no wash” experiments. For nuclear staining, cells were incubated in PBS for 5 min (2 \times), and then incubated in PBS containing 5 μM DRAQ5 (Cell Signaling) for 5 min, followed by brief wash with PBS (1 \times). During all imaging experiments, cells were maintained at 37 °C in a humidified 5% CO₂ v/v environment supplied by a live-cell incubator (TOKAI HIT).

Microscopy Hardware

Three separate systems were used to acquire microscopic images. Confocal microscopy was performed using a Zeiss LSM 510 META confocal microscope with a LD C-APOCHROMAT 40 \times /1.2 W Korr M27 UV-VIS-IR objective. Wide-field microscopy, 2D single-molecule tracking, and super-resolution imaging experiments were conducted on a Nikon Eclipse Ti wide field epifluorescence microscope equipped with a 100 \times , 1.4NA oil-immersion objective lens (Nikon), a Lumencor light source, a set of lasers (405 nm/100 mW, Coherent Cube; 561 nm/200 mW, Cobolt Jive; 633 nm/140 mW, Vortran Stradus), controlled by an Acousto-Optic Tunable Filter (AA Opto-Electronic), two filter wheels (Lambda 10-3; Sutter Instruments), a perfect focusing system (Nikon), and an EMCCD camera (iXon3, Andor). Emission filters (FF01 593/40 or FF01 676/37; Semrock) were placed in front of the cameras for JF₅₄₉ and JF₆₄₆ emission. A multi-band mirror (405/488/561/633 BrightLine quad-band bandpass filter, Semrock) was used to reflect the excitation laser beams into the objective. The microscope, cameras, and hardware were controlled through the NIS-Elements software (Nikon). Other live-cell single super-resolution imaging experiments were recorded on a custom-built three-camera RAMM

frame (ASI) microscope using an 1.4NA PLAPON 60× OSC objective (Olympus), and a 300 mm focal length tube lens (LAO-300.0, Melles Griot), resulting in 100× overall magnification. Stroboscopic 405 nm excitation of the Stradus 405-100 laser (Vortran) was achieved using a NI-DAQ-USB-6363 acquisition board (National Instruments), which also controlled the 637 nm laser emission from a Stradus 637-140 laser (Vortran). A 2mm-thick quad-band dichroic (ZT 405/488/561/640rpx, Chroma), and a band-pass emission filter (FF01-731/137-25, Semrock) filtered the emitted light. Fluorescence was detected with a back-illuminated EMCCD camera (Andor Technology, Ixon Ultra DU-897U-CS0-EXF, 17 MHz EM amplifier), which was controlled through Micro-Manager (1.4.17).

dSTORM Imaging

Super-resolution imaging experiments were performed on live samples (Fig. 2j, Supplementary Fig. 2c, Supplementary Fig. 4d, Supplementary Fig. 4g) and fixed cells (Fig. 1i, Fig. 2b, Supplementary Fig. 2a, Supplementary Fig. 4a). For live-cell dSTORM imaging the cells were labeled, washed, and imaged directly in DMEM–FBS. For fixed cell preparations, cells were labeled, washed, and fixed in 4% paraformaldehyde (Electron Microscopy Sciences) in PBS buffer (pH = 7.5). The cells were imaged in a sealed cell chamber (Life Technologies) containing nitrogen-degassed redox buffer consisting of PBS supplemented with 50 mM mercaptoethylamine (Sigma–Aldrich), 10% w/v glucose, 0.5 mg/mL glucose oxidase (Sigma–Aldrich), and 28400 U/mL catalase (Sigma–Aldrich). Before imaging, JF₅₄₉ could be efficiently “shelved” in a dark state upon illumination with 2 kW·cm⁻² of excitation light (561 nm), and then activated back to a fluorescent state by blue light (405 nm) with low intensity (~20·W cm⁻²). JF₆₄₆ fluorophores were converted into a predominately dark state using continuous illumination of 637 nm excitation light at 14 kW·cm⁻², after which individual rapidly blinking molecules of JF₆₄₆ fluorophores were observed. These experiments were conducted on the two wide-field microscope systems described above: the Nikon Eclipse Ti epifluorescence microscope (Fig. 1i, Fig. 2j, Supplementary Fig. 2a, Supplementary Fig. 2c, Supplementary Fig. 4g), and the custom-built three-camera microscope with an ASI RAMM frame (Fig. 2b, Supplementary Fig. 4a, Supplementary Fig. 4d).

dSTORM Analysis

The spot localization (x, y) was obtained based on the multiple-target tracing (MTT) algorithm^{46,47} using a custom MATLAB program. For each frame, the PSF of individual fluorophores was fitted into a two-dimensional Gaussian distribution. Integrated fluorescence intensities were calculated and converted to photon counts using analysis routines written in IGOR Pro version 6.34A. Localization errors were calculated using Equation 6 in Mortensen *et al.*⁴⁸ Super-resolution images were rendered using the software package Localizer by Dedecker *et al.*⁴⁹ running from Igor Pro v. 3.34A, which superimposes the position coordinates of detected spots as Gaussian masks using the fitted intensity values as amplitudes and the localization errors as the widths. The dSTORM data for experiments comparing two different fluorophore ligands was recorded on the same day under identical illumination conditions.

Two-Color Single-Molecule Experiments

The two-color single-molecule experiments were recorded on the Nikon Eclipse Ti wide field epifluorescence microscope. We first performed a 2D single molecule tracking of SnapTag–TetR–JF₅₄₉ using a 561-nm laser of excitation intensity $\sim 1 \text{ kW cm}^{-2}$ at a frame rate of 100 Hz. Immediately after the completion of the single-particle tracking experiment, we then imaged HaloTag–H2B–JF₆₄₆ under the *d*STORM mode as described above. Transmission images were taken before and after the tracking–*d*STORM experiments and a cross-correlation algorithm was employed to calculate the image drift.⁵⁰ Tracking analysis of TetR was performed using the commercial tracking software DiaTrack (v. 3.03, Semasopt), which identifies and fits the intensity spots of fluorescent particles with 2D Gaussian functions matched to the experimentally determined point-spread function. The diffusion map was created using tracking routines written in IGOR Pro 6.34A, calculating the local apparent diffusion of TetR mobility evaluated on a $20 \text{ nm} \times 20 \text{ nm}$ x–y grid from the mean square displacements over a timescale of 10 milliseconds (Fig. 2j). Whenever two or more separate displacements originating within 80 nm of a given grid node were found, a local apparent diffusion coefficient was calculated and plotted. We then selected H2B clusters as the 500 brightest spots in the super-resolved image. From this analysis, we generated a histogram of apparent diffusion coefficients for all trajectories that dwelled within 320 nm of a H2B cluster for at least 10 milliseconds. We then plotted histograms of the diffusion coefficient of both the H2B-colocalized and the non-colocalized TetR trajectories (Supplementary Fig. 4h).

Supplementary Material

Refer to Web version on PubMed Central for supplementary material.

Acknowledgments

We thank S. Eddy and E. Betzig for contributive discussions, M. Dahan (Curie Institut) and X. Darzacq (Berkeley) for the SnapTag–TetR plasmid, M. Tadross (Janelia) for the purified HaloTag protein, and W. Hu (Janelia) for cloning and purifying the recombinant HaloTag–MS2 protein. This work was supported by the Howard Hughes Medical Institute. Salary for R.H.S. is funded by US National Institutes of Health grants GM57071, NS83085, and EB13571.

References

1. Kremers GJ, Gilbert SG, Cranfill PJ, Davidson MW, Piston DW. Fluorescent proteins at a glance. *J Cell Sci.* 2011; 124:157–160. [PubMed: 21187342]
2. Xia T, Li N, Fang X. Single-molecule fluorescence imaging in living cells. *Ann Review Phys Chem.* 2013; 64:459–480.
3. Griffin BA, Adams SR, Tsien RY. Specific covalent labeling of recombinant protein molecules inside live cells. *Science.* 1998; 281:269–272. [PubMed: 9657724]
4. Keppler A, et al. A general method for the covalent labeling of fusion proteins with small molecules in vivo. *Nat Biotechnol.* 2002; 21:86–89. [PubMed: 12469133]
5. Los GV, et al. HaloTag: A novel protein labeling technology for cell imaging and protein analysis. *ACS Chem Biol.* 2008; 3:373–382. [PubMed: 18533659]
6. Encell LP, et al. Development of a dehalogenase-based protein fusion tag capable of rapid, selective and covalent attachment to customizable ligands. *Curr Chem Genomics.* 2012; 6(Suppl 1-M7):55–71. [PubMed: 23248739]

7. Wombacher R, et al. Live-cell super-resolution imaging with trimethoprim conjugates. *Nat Methods*. 2010; 7:717–719. [PubMed: 20693998]
8. Hori Y, Ueno H, Mizukami S, Kikuchi K. Photoactive yellow protein-based protein labeling system with turn-on fluorescence intensity. *J Am Chem Soc*. 2009; 131:16610–16611. [PubMed: 19877615]
9. Uttamapinant C, et al. A fluorophore ligase for site-specific protein labeling inside living cells. *Proc Natl Acad Sci USA*. 2010; 107:10914–10919. [PubMed: 20534555]
10. Testa I, et al. Multicolor fluorescence nanoscopy in fixed and living cells by exciting conventional fluorophores with a single wavelength. *Biophys J*. 2010; 99:2686–2694. [PubMed: 20959110]
11. Zhao ZW, et al. Spatial organization of RNA polymerase II inside a mammalian cell nucleus revealed by reflected light-sheet superresolution microscopy. *Proc Natl Acad Sci USA*. 2014; 111:681–686. [PubMed: 24379392]
12. Abrahamsson S, et al. Fast multicolor 3D imaging using aberration-corrected multifocus microscopy. *Nat Methods*. 2013; 10:60–63. [PubMed: 23223154]
13. Chen J, et al. Single-molecule dynamics of enhanceosome assembly in embryonic stem cells. *Cell*. 2014; 156:1274–1285. [PubMed: 24630727]
14. Lavis LD, Raines RT. Bright ideas for chemical biology. *ACS Chem Biol*. 2008; 3:142–155. [PubMed: 18355003]
15. Beija M, Afonso CAM, Martinho JMG. Synthesis and applications of rhodamine derivatives as fluorescent probes. *Chem Soc Rev*. 2009; 38:2410–2433. [PubMed: 19623358]
16. Lavis LD, Raines RT. Bright building blocks for chemical biology. *ACS Chem Biol*. 2014; 9:855–866. [PubMed: 24579725]
17. Gautier A, et al. An engineered protein tag for multiprotein labeling in living cells. *Chem Biol*. 2008; 15:128–136. [PubMed: 18291317]
18. Lukinavičius G, et al. A near-infrared fluorophore for live-cell super-resolution microscopy of cellular proteins. *Nature Chem*. 2013; 5:132–139. [PubMed: 23344448]
19. Mujumdar RB, Ernst LA, Mujumdar SR, Lewis CJ, Waggoner AS. Cyanine dye labeling reagents: Sulfoindocyanine succinimidyl esters. *Bioconjugate Chem*. 1993; 4:105–111.
20. Panchuk-Voloshina N, et al. Alexa Dyes, a series of new fluorescent dyes that yield exceptionally bright, photostable conjugates. *J Histochem Cytochem*. 1999; 47:1179–1188. [PubMed: 10449539]
21. Haugland, RP.; Spence, MTZ.; Johnson, ID.; Basey, A. *The Handbook: A Guide to Fluorescent Probes and Labeling Technologies*. 10. Molecular Probes; 2005.
22. Zhang Z, Revyakin A, Grimm JB, Lavis LD, Tjian R. Single-molecule tracking of the transcription cycle by sub-second RNA detection. *eLife*. 2014; 3:e01775. [PubMed: 24473079]
23. Bosch PJ, et al. Evaluation of fluorophores to label SNAP-tag fused proteins for multicolor single-molecule tracking microscopy in live cells. *Biophys J*. 2014; 107:803–814. [PubMed: 25140415]
24. Grimm JB, et al. Carbofluoresceins and carborhodamines as scaffolds for high-contrast fluorogenic probes. *ACS Chem Biol*. 2013; 8:1303–1310. [PubMed: 23557713]
25. Vogel M, Rettig W, Sens R, Drexhage KH. Structural relaxation of rhodamine dyes with different *N*-substitution patterns—a study of fluorescence decay times and quantum yields. *Chem Phys Lett*. 1988; 147:452–460.
26. Grabowski ZR, Rotkiewicz K, Rettig W. Structural changes accompanying intramolecular electron transfer: Focus on twisted intramolecular charge-transfer states and structures. *Chem Rev*. 2003; 103:3899–4032. [PubMed: 14531716]
27. Song X, Johnson A, Foley J. 7-Azabicyclo[2.2.1]heptane as a unique and effective dialkylamino auxochrome moiety: Demonstration in a fluorescent rhodamine dye. *J Am Chem Soc*. 2008; 130:17652–17653. [PubMed: 19108696]
28. Grimm JB, Lavis LD. Synthesis of rhodamines from fluoresceins using Pd-catalyzed C–N cross-coupling. *Org Lett*. 2011; 13:6354–6357. [PubMed: 22091952]
29. Heilemann M, et al. Subdiffraction-resolution fluorescence imaging with conventional fluorescent probes. *Angew Chem Int Ed*. 2008; 47:6172–6176.

30. Dempsey GT, Vaughan JC, Chen KH, Bates M, Zhuang X. Evaluation of fluorophores for optimal performance in localization-based super-resolution imaging. *Nat Methods*. 2011; 8:1027–1036. [PubMed: 22056676]
31. Ha T, Tinnefeld P. Photophysics of fluorescence probes for single molecule biophysics and super-resolution imaging. *Annu Rev Phys Chem*. 2012; 63:595–617. [PubMed: 22404588]
32. Lukinavičius G, et al. Fluorogenic probes for live-cell imaging of the cytoskeleton. *Nat Methods*. 2014; 11:731–733. [PubMed: 24859753]
33. Loving G, Imperiali B. A versatile amino acid analogue of the solvatochromic fluorophore 4-*N,N*-dimethylamino-1,8-naphthalimide: A powerful tool for the study of dynamic protein interactions. *J Am Chem Soc*. 2008; 130:13630–13638. [PubMed: 18808123]
34. Kubota Y, Steiner RF. Fluorescence decay and quantum yield characteristics of acridine orange and proflavine bound to DNA. *Biophys Chem*. 1977; 6:279–289. [PubMed: 880342]
35. Lee LG, Berry GM, Chen CH. Vita Blue: A new 633-nm excitable fluorescent dye for cell analysis. *Cytometry*. 1989; 10:151–164. [PubMed: 2714106]
36. Bancaud A, et al. Molecular crowding affects diffusion and binding of nuclear proteins in heterochromatin and reveals the fractal organization of chromatin. *EMBO J*. 2009; 28:3785–3798. [PubMed: 19927119]
37. Bancaud A, Lavelle C, Huet S, Ellenberg J. A fractal model for nuclear organization: Current evidence and biological implications. *Nucleic Acids Res*. 2012; 40:8783–8792. [PubMed: 22790985]
38. Speight LC, et al. Efficient synthesis and in vivo incorporation of acridon-2-ylalanine, a fluorescent amino acid for lifetime and Förster resonance energy transfer/luminescence resonance energy transfer studies. *J Am Chem Soc*. 2013; 135:18806–18814. [PubMed: 24303933]
39. Mitronova GY, et al. New fluorinated rhodamines for optical microscopy and nanoscopy. *Chem Eur J*. 2010; 16:4477–4488. [PubMed: 20309973]
40. Altman RB, et al. Cyanine fluorophore derivatives with enhanced photostability. *Nat Methods*. 2012; 9:68–71. [PubMed: 22081126]
41. Suzuki K, et al. Reevaluation of absolute luminescence quantum yields of standard solutions using a spectrometer with an integrating sphere and a back-thinned CCD detector. *Phys Chem Chem Phys*. 2009; 11:9850–9860. [PubMed: 19851565]
42. Critchfield FE, Gibson JA Jr, Hall JL. Dielectric constant for the dioxane–water system from 20 to 35°. *J Am Chem Soc*. 1953; 75:1991–1992.
43. Mütze J, et al. Excitation spectra and brightness optimization of two-photon excited probes. *Biophys J*. 2012; 102:934–944. [PubMed: 22385865]
44. Akerboom J, et al. Optimization of a GCaMP calcium indicator for neural activity imaging. *J Neurosci*. 2012; 32:13819–13840. [PubMed: 23035093]
45. Magde D, Rojas GE, Seybold PG. Solvent dependence of the fluorescence lifetimes of xanthene dyes. *Photochem Photobiol*. 1999; 70:737–744.
46. Serge A, Bertaux N, Rigneault H, Marguet D. Multiple-target tracing (MTT) algorithm probes molecular dynamics at cell surface. *Nature Protocol Exchange*. 2008.10.1038/nprot.2008.1128
47. Serge A, Bertaux N, Rigneault H, Marguet D. Dynamic multiple-target tracing to probe spatiotemporal cartography of cell membranes. *Nat Methods*. 2008; 5:687–694. [PubMed: 18604216]
48. Mortensen KI, Churchman LS, Spudich JA, Flyvbjerg H. Optimized localization analysis for single-molecule tracking and super-resolution microscopy. *Nat Methods*. 2010; 7:377–381. [PubMed: 20364147]
49. Dedecker P, Duwé S, Neely RK, Zhang J. Localizer: Fast, accurate, open-source, and modular software package for superresolution microscopy. *J Biomed Opt*. 2012; 17:126008–126008. [PubMed: 23208219]
50. Guizar-Sicairos M, Thurman ST, Fienup JR. Efficient subpixel image registration algorithms. *Opt Lett*. 2008; 33:156–158. [PubMed: 18197224]

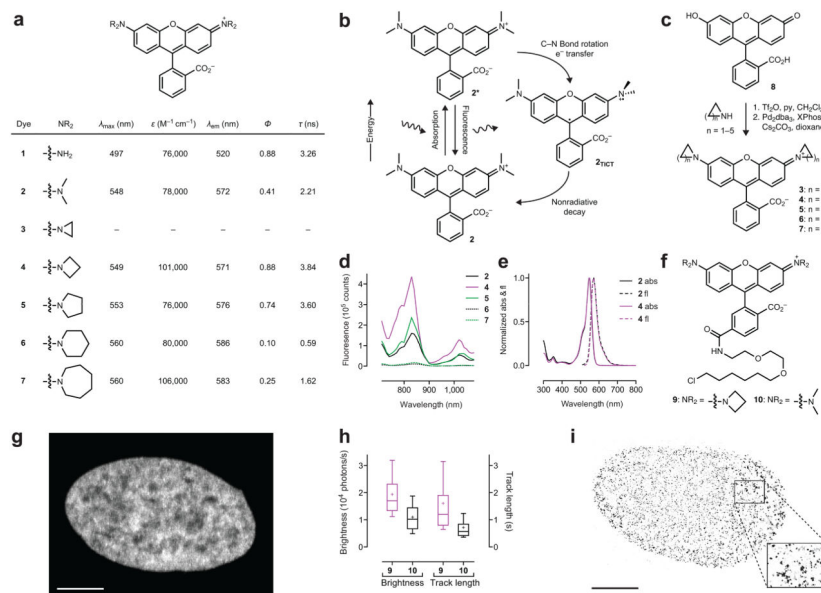


Figure 1. Development and utility of JF549

(a) Spectroscopic data for rhodamines 1–7. (b) Jablonski diagram showing the process of twisted internal charge transfer (TICT). (c) Synthesis of rhodamines 3–7 from fluorescein (8) using Pd-catalyzed cross-coupling. (d) Two-photon excitation spectra of fluorophores 2, 4–7. (e) Normalized absorption (abs) and fluorescence emission (fl) spectra for tetramethylrhodamine (2) and JF549 (4). (f) Chemical structure of JF549–HaloTag ligand 9 and TMR–HaloTag ligand 10. (g) Confocal maximum projection image of nucleus from a live, washed HeLa cell expressing HaloTag–H2B and incubated with JF549–HaloTag ligand 9; scale bar = 5 μ m. (h) Whisker plot comparing brightness and track length of HaloTag–H2B molecules labeled with ligand 9 or 10 ($n > 4,000$); cross indicates mean; whiskers span 10–90 percentile. (i) *d*STORM fluorescence microscopy image of a fixed U2OS cell expressing HaloTag–H2B and labeled with JF549 ligand 9. The *d*STORM image is comprised of 10,000 consecutive frames and the 44,937 detected particles are displayed according to their localization FWHM. The mean localization error was 17.2 nm, the median localization error was 14.1 nm; scale bar = 5 μ m.

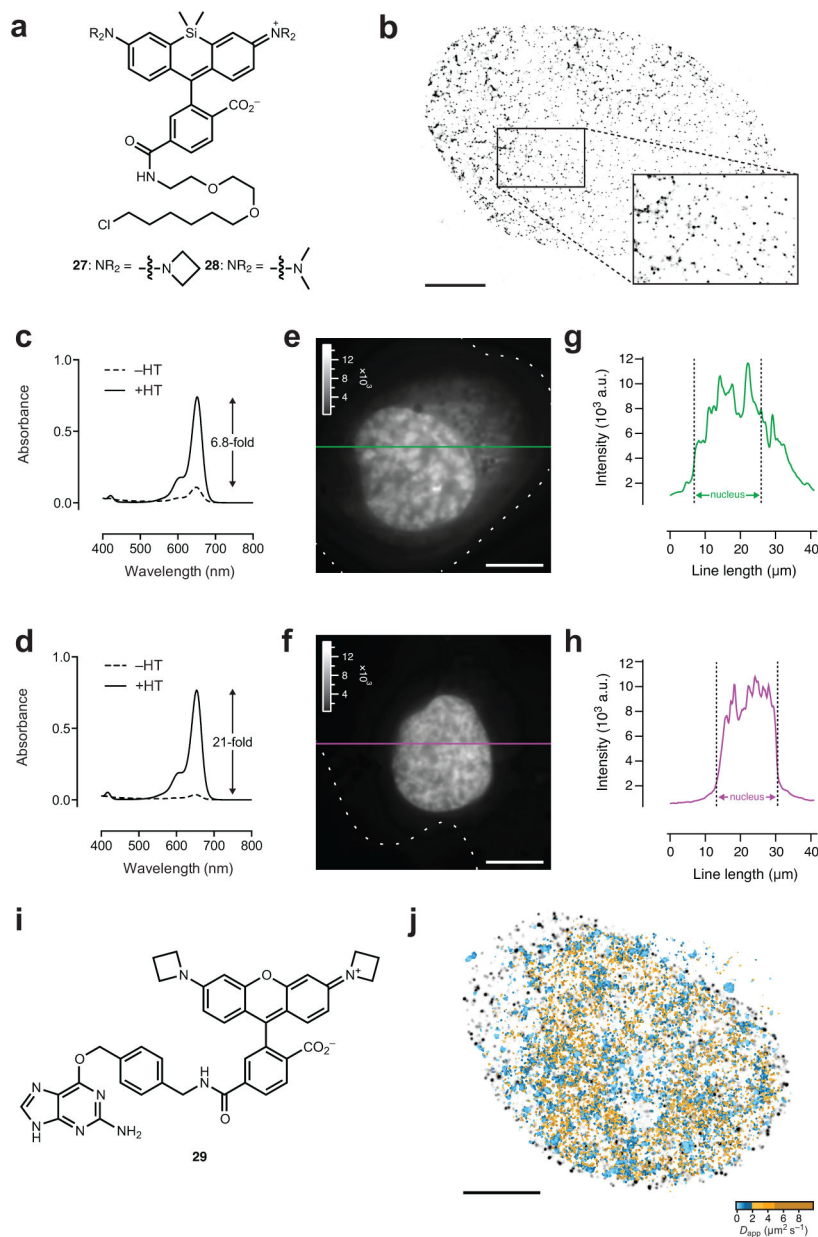


Figure 2. Utility of JF₆₄₆ in cellular imaging

(a) Chemical structures of JF₆₄₆-HaloTag ligand **27** and SiTMR-HaloTag ligand **28**. (b) *d*STORM fluorescence microscopy image of fixed U2OS cells expressing HaloTag-H2B and labeled with **27**. The *d*STORM image is comprised of 5,000 consecutive frames and the 263,415 detected particles are displayed according to their localization FWHM. The mean localization error was 11.1 nm, the median localization error was 8.4 nm; scale bar = 5 μm. (c, d) Absorbance spectra of ligands **28** (5 μM; c) and **27** (5 μM; d) in the absence (-HT) and presence (+HT) of excess HaloTag protein. (e, f) Wide-field fluorescence microscopy image of a live HeLa cell transfected with H2B-HaloTag, incubated with **28** (100 nM; e) or **27** (100 nM; f), and imaged without intermediate washing steps; dashed line indicates cellular boundary; scale bars: 5 μm. (g) Plot of line scan intensity in e (green) as a function

of line length. **(h)** Plot of line scan intensity in **f** (magenta) as a function of line length. **(i)** Chemical structure of JF₅₄₉-SnapTag ligand **29**. **(j)** Overlay of the *d*STORM image of H2B and regions of fast TetR diffusivity (2–10 $\mu\text{m}^2 \text{s}^{-1}$; yellow) and slow TetR diffusivity (<2 $\mu\text{m}^2 \text{s}^{-1}$; blue).

Author Manuscript

Author Manuscript

Author Manuscript

Author Manuscript

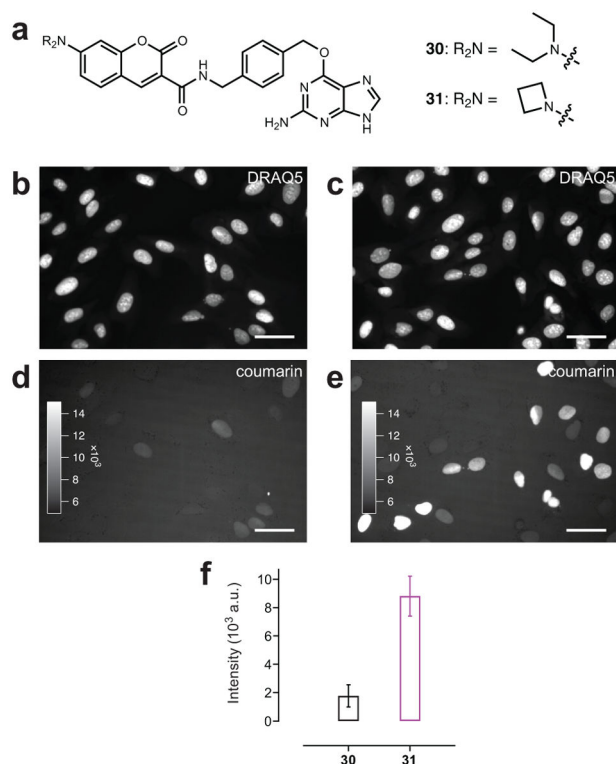
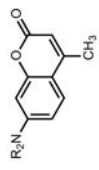
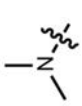

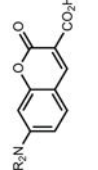


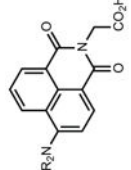
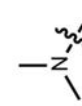

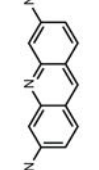
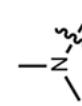



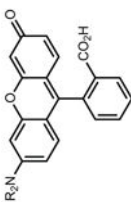

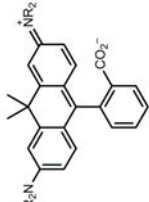

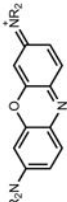

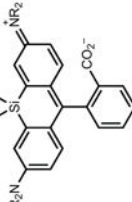

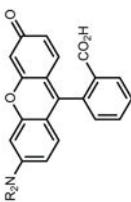

Figure 3. Utility of azetidiny coumarins in cellular imaging

(a) Chemical structures of commercial coumarin SnapTag ligand **30** and azetidine-containing ligand **31**. (b, d) Wide-field fluorescence microscopy images of live HeLa cells expressing SnapTag-H2B and labeled with DRAQ5 and commercial SnapTag ligand **30**. (b) Fluorescence of DRAQ5 nuclear staining. (d) Fluorescence of coumarin **30**-labeled SnapTag-H2B. (c, e) Wide-field fluorescence microscopy image of live HeLa cells expressing SnapTag-H2B and labeled with DRAQ5 and novel azetidiny-coumarin SnapTag ligand **31**. (c) Fluorescence of DRAQ5 nuclear staining. (e) Fluorescence of coumarin **31**-labeled SnapTag-H2B. Scale bars for all images: 50 μm . (f) Quantification of the average nuclear fluorescence above background coumarin label in cells when labeled with ligand **30** (black) or **31** (magenta; error bars show s.e.m.).

Table 1

Spectroscopic data for fluorophores 11–26

Parent structure	Substitution	λ_{max} (nm)	ϵ (M ⁻¹ cm ⁻¹)	λ_{em} (nm)	Φ
		372	18,000	470	0.19
		354	15,000	467	0.96
		410	35,000	471	0.03
		387	24,000	470	0.84
		436	9,500	–	<0.01
		464	18,000	553	0.28
		493	50,000	528	0.21
		492	47,000	531	0.52

Parent structure	Substitution	λ_{max} (nm)	ϵ ($\text{M}^{-1} \text{cm}^{-1}$)	λ_{em} (nm)	Φ
		518	60,000	546	0.21
		606	121,000	626	0.52
		655	111,000	669	0.07
		643	141,000 ^d	662	0.41
		646	152,000 ^d	664	0.54

^d Extinction coefficient measured in ethanol containing 0.1% v/v trifluoroacetic acid